Int J Adv Manuf Technol (2017) 93:1669–1683
DOI 10.1007/s00170-017-0661-y

ORIGINAL ARTICLE

Kinematic modeling and deformation mechanics in shot peening of functional ceramics

Z. Y. Liu[1] · C. Huang[2] · Y. Zhao[3] · Y. B. Guo[1]

Received: 10 February 2017 / Accepted: 7 June 2017 / Published online: 21 June 2017

Abstract The applications of functional ceramics are significantly limited by the brittleness and low reliability. Recent studies have shown that compressive residual stress can be created in ceramics by shot peening, which improves the contact strength and fatigue of ceramic components. However, the formation mechanism of residuals stress in shot peening is yet to understand. In this study, a pressure-dependent plasticity model has been incorporated into a finite element simulation model of shot peening to understand the process mechanism underpinning the residual stress formation. Since shot velocity is the key process parameter to dominate the impact energy which determines the deformation state of the peened surface and the resultant residual stress, a new kinematic model of shots has also been developed by incorporating air drag and travel distance inside and outside the peening nozzle. The results have shown that the shot velocity model can be used to predict shot velocity. The experiment-based model may help understand the process mechanism underpinning the residual stress formation.

Keywords Shot peening · Residual stress · Ceramics plasticity · Almen intensity · Finite element simulation

✉ Y. B. Guo
yguo@eng.ua.edu

[1] Department of Mechanical Engineering, The University of Alabama, Tuscaloosa, AL 35487, USA

[2] School of Mechanical Engineering, Shandong University, Jinan, Shandong 250061, China

[3] Institute for Advanced Manufacturing, Shandong University of Technology, Zibo 255049, China

Nomenclature

F_D	Drag force
C_D	Drag coefficient
A_s	Cross-section area of the shot
ρ_a^n	Density of the compressed air in nozzle
v_a^n	Air flow velocity in nozzle
v_s	Velocity of the shot
R_i	Individual gas constants
v_L	Air velocity limit
m_s	Shot mass
d_s	Shot diameter
ρ_s	Shot density
a_s	Shot acceleration
l_n	Nozzle length
x	Distance between shot and nozzle exit
d_n	Diameter of the nozzle
v_a^x	Air velocity after leaving the nozzle
ρ_a^x	Air density after leaving nozzle
l_s	Length of computational segment
σ_i^*	Normalized intact equivalent stress
HEL	Hugoniot elastic limit
σ_{HEL}	Equivalent stress at HEL
D	Damage variable
σ^*	Normalized equivalent stress
P_{HEL}	Pressure at the HEL
P^*	Normalized pressure
T^*	Normalized maximum tensile hydrostatic pressure
T	Maximum tensile hydrostatic pressure
$\dot{\varepsilon}^*$	Dimensionless strain rate
$\dot{\varepsilon}_0$	Reference strain rate
ε_p^f	Equivalent plastic strain to fracture
D_1	Parameter for plastic strain to fracture
D_2	Parameter for plastic strain to fracture (exponent)
K_1	Bulk modulus
K_2	Second pressure coefficient

K_3 Third pressure coefficient
B Fraction of the elastic energy loss converted to potential hydrostatic energy

1 Introduction

The excellent wear resistance and high temperature strength of ceramics allow their wide applications in bearing, gas turbines, cutting tools, and medical devices [1]. However, ceramics are intrinsically brittle due to the nature of the ionic and covalent bonding. Shot peening is a mechanical surface treatment process to improve fatigue life of aerospace and automobile metallic components by introducing a compressive residual stress in surface layer. It was believed for a long time that ceramic strengthening by shot peening would be impossible since these brittle materials have been assumed to tolerate little plastic deformation by mechanical loading. However, a few recent studies have shown that the near-surface strength of ceramics can be improved by shot peening [2–6]. High compressive residual stress was introduced into the near surface in ceramics by shot peening. Furthermore, contact strength and fatigue performance of ceramics can be improved because of the compressive residual stresses [5].

1.1 Shot peening of ceramics

Pfeiffer et al. have investigated residual stress in shot peened alumina and silicon nitride. Compressive residual stress up to −1 GPa can be introduced into the surface to increase surface strength [5]. The influence of shot peening process parameters on the residual stress state, dislocation density, surface topography, and the static, cyclic, and rolling near-surface strength was determined. Moon et al. observed high density of dislocations and micro-cracks in the sub-surface using TEM [3]. Tanaka et al. reported that compressive residual stress up to −1.5 GPa was introduced into the near-surface of shot peened Si_3N_4 samples [7]. Takahashi et al. investigated the combination effects of shot peening and crack-healing on residual stress, apparent fracture toughness, and the Weibull distribution of the contact strength of ceramics. It was found that shot peening was effective to increase the contact strength and decrease the scatter of the contact strength [6, 8].

1.2 Shot velocity

Shot velocity dominates its kinematic energy which in turn dominates the impact energy in shot peening, therefore, determines the magnitude and depth of residual stress. An insightful understanding of the influencing process parameter of shot velocity is essential to the control of a shot peening process, in which a shot is introduced into the nozzle and accelerated by the compressed air flow. When the shot exits the nozzle, the air velocity is higher than the shot velocity. The shot is accelerated at first. However, the air density and velocity will decrease after leaving the nozzle. When the air velocity is lower than the shot velocity, the shot velocity will be decreased. Kirk developed the first model to calculate shot velocity considering only the acceleration stage when the shot is still in the nozzle [9]. Another limitation of Kirk's model is that an approximation method was employed to obtain the numerical solution. Similar to the Kirk's model, Li et al. have developed a particle velocity model for abrasive air jet to consider the particle velocity evolution when particle is outside the nozzle [10]. A numerical solution to solve the particle acceleration equation was also developed. However, the air density variation after leaving the nozzle was not considered.

Intensity is the key parameter in shot peening to characterize the amount of kinematic energy of shot to workpiece deformation energy. The method commonly used to quantify the intensity was developed by Almen and Black [11]. They created Almen strip to measure the compressive residual stress induced by shot peening operation. Almen intensity can be obtained by measuring the deformation of Almen strip. Almen intensity provides an easy way to determine the intensity of shot steam. Thus, it is widely used to the control of a shot peening process. Great efforts have been devoted to relate the shot peening process parameters to Almen intensity. Miao et al. developed an analytical approach to predict Almen intensity. The predicted results are in good agreement with the experimental results [12]. However, all those models require the shot velocity as a critical input parameter.

1.3 Finite element analysis (FEA) of shot peening

Due to the complexity of a shot peening process, it is beyond the capability of conventional analytical method to provide insight into the microscale mechanical behavior of ceramics in shot peening. With the development of the finite element method and the rapid development of computational power, FEA of shot peening process has been conducted. Al-Obaid developed the first FE model of shot peening in 1990 [13]. The predicted residual stress distributions were in good agreement with results in literatures. Subsequently, a series of finite element analysis have been performed to simulate various shot peening processes. A lot efforts have been devoted to develop FE models to simulate shot peening more realistically, such as FE models with multiple impacts at different locations [14, 15], different impact angles [16], and random multiple peening [17]. While most studies focus on the prediction of residual stress, Frija et al. investigated the damage induced by shot peening with FEA by incorporating an elastic-plastic-damage material model [18]. Bagherifard et al. studied surface roughness induced by shot peening with FEA [19]. Gangaraj et al. developed a random FE model to investigate the coverage of shot peening process [20]. However, all those

simulations were focused on the mechanical behavior of metals in shot peening. No report on FEA of shot peening of ceramics can be found in literature.

1.4 Research objectives

Current studies on shot peening of ceramics are limited to experiments and lack of theoretical studies. The formation mechanism of residual stress in ceramics introduced by shot peening has not been investigated yet. The formation of residual stress indicates the occurrence of plastic deformation, which has not been well understood. A fundamental study of mechanical behavior of ceramics in peening is critical to understand the microsacle plastic deformation phenomena.

In this work, a pressure-dependent plasticity model was incorporated into a FE model to investigate the mechanical behavior of ceramics in peening and shed light on the residual stress formation mechanism. A new kinematic model of shot was developed to calculate shot velocity by incorporating the air flow density change outside of the nozzle. The shot velocity determined by the new shot velocity model was then input as an initial condition of the FE model.

2 Kinematic model and numerical implementation with air drag and density variation

2.1 Shot velocity inside the nozzle

The peening shot moving through a nozzle is accelerated by the air stream because of the drag force imposed by fast flowing air stream as shown in Fig. 1.

The drag force F_D is regarded to be proportional to the square of the velocity difference between the air flow and the shot.

$$F_D = \frac{1}{2} C_D A_s \rho_a^n \left(v_a^n - v_s\right)^2 \tag{1}$$

where C_D is the "drag coefficient" (a dimensionless number that depends upon the shape of the object and for a smooth sphere $C_D \approx 0.5$). The collisions between the shots were neglected in this study for simplicity.

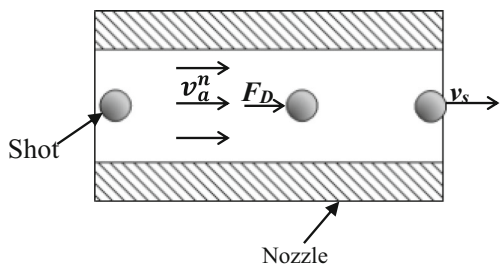

Fig. 1 Shot acceleration in the nozzle

Based on the Bernoulli equation for compressible flow as a function of the pressure ratio, the air flow velocity v_a^n in nozzle can be given by [21]

$$v_a^n = \left(2 \frac{\kappa}{\kappa - 1} \frac{p}{\rho_a^n} \left[1 - \left(\frac{p_0}{p} \right)^{(\kappa-1)/\kappa} \right] \right)^{1/2} \tag{2}$$

where κ is the adiabatic exponent that takes a value of 1.4 for air, p is the absolute air pressure in nozzle, and p_0 is the atmospheric pressure. The air density ρ_a^n in the nozzle depends on the air pressure and temperature with the following relationship

$$\rho_a^n = \frac{p}{R_i T} \tag{3}$$

where R_i is the individual gas constants with a value of 287 N m/(kg K) and T is the absolute temperature.

For a cylindrical nozzle, there exists an air velocity limit v_L that cannot be exceeded which is given by [22]

$$v_L = \left(2 \frac{\kappa}{\kappa + 1} R_i T \right)^{1/2} \tag{4}$$

The acceleration of shots through a nozzle is governed by the Newton's second law of motion (Eq. 5). The cross section area A_s and shot mass m_s can be given by Eqs. 6 and 7.

$$\frac{dv_s}{dt} = \frac{C_D A_s \rho_a^n \left(v_a^n - v_s\right)^2}{2 m_s} \tag{5}$$

$$A_s = \frac{\pi d_s^2}{4} \tag{6}$$

$$m_s = \frac{\pi d_s^3 \rho_s}{6} \tag{7}$$

where d_s and ρ_s are the diameter and density of a shot, respectively.

Combining Eqs. 1–7, the shot acceleration a_s can be calculated by Eq. 8. Under the approximation of constant acceleration over the nozzle length l_n, Eq. 9 was derived from Eq. 8 and the work-energy theorem [9]. Shot velocity v_s can be estimated by solving Eq. 9.

$$a_s = \frac{dv_s}{dt} = \frac{3 C_D \rho_a^n \left(v_a^n - v_s\right)^2}{4 d_s \rho_s} \tag{8}$$

$$v_s = \left(\frac{3 C_D \rho_a^n l_n}{2 \rho_s d_s} \right)^{1/2} \left(v_a^n - v_s\right) \tag{9}$$

2.2 Modeling of shot velocity outside the nozzle

The evolution of the air flow after leaving nozzle can be divided into two regions, the initial region and the main region as shown in Fig. 2. It is regarded that the center line velocity in the initial region equals to air velocity v_a^n in the nozzle while the center line velocity in the main region is proportional to $1/x$. According to Rajaratnam [23], the center line air velocity v_a^x after leaving the nozzle can be expressed by

$$v_a^x = \begin{cases} v_a^n & x \le 6.2d_n \\ v_a^n\left(\dfrac{6.2d_n}{x}\right) & x > 6.2d_n \end{cases} \tag{10}$$

where d_n is the diameter of the nozzle, x is the axial distance from the nozzle exit.

It should be noted that the air density will decrease after leaving the nozzle exit due to the flow expansion. It is difficult to determine the density variation by experiment. To get a more realistic result, an assumption that air density ρ_a^x after leaving nozzle decreases at an exponential rate can be expressed by

$$\rho_a^x = Ae^{-Bx} + C \tag{11}$$

where B is the decay rate of air density after leaving nozzle.

The boundary conditions are given by Eq. 12, where ρ_a^0 is the density of atmosphere air, then A and C can be obtained by Eq. 13. Assume that the air flow density at the peening target decreases to $\alpha\rho_a^n$, i.e., Eq. 14, where l is the distance between nozzle to the peening target, then B can be solved by Eq. 15. In addition, the air density after leaving the nozzle can be expressed as Eq. 16.

$$\begin{cases} \rho_a^x = \rho_a^n & x = 0 \\ \rho_a^x = \rho_a^0 & x \to +\infty \end{cases} \tag{12}$$

$$\begin{cases} A = \rho_a^n - \rho_a^0 \\ C = \rho_a^0 \end{cases} \tag{13}$$

$$\rho_a^x\big|_{x=l} = Ae^{-Bl} + C = \alpha\rho_a^n \tag{14}$$

$$B = \frac{1}{l} ln\frac{\rho_a^n - \rho_a^0}{\alpha\rho_a^n - \rho_a^0} \tag{15}$$

$$\rho_a^x = \left(\rho_a^n - \rho_a^0\right)e^{\frac{x}{l}ln\frac{\alpha\rho_a^n - \rho_a^0}{\rho_a^n - \rho_a^0}} + \rho_a^0 \tag{16}$$

2.3 Numerical implementation and discussions

To obtain a practical solution of shot velocity, a numerical approach is developed in this study based on the previous work given by Li et al. [10]. The nozzle length is divided into n identical small segments of length $l_s = l/n$. Within each segment, the shot acceleration is assumed to be constant, and the relative velocity $\left(v_a^n - v_s\right)$ can be calculated using the shot velocity at the start point of the segment.

$$\left(v_s^i\right)^2 - \left(v_s^{i-1}\right)^2 = 2a_s^i l_s \tag{17}$$

$$v_s^i = \left[\left(v_s^{i-1}\right)^2 + \frac{3l_s C_d \rho_a^n}{2\rho_s d_s}\left(v_a^n - v_s^{i-1}\right)^2\right]^{1/2} \tag{18}$$

Similar to Eq. 18, the shot velocity v_s^i after leaving the nozzle is given by

$$v_s^i = \begin{cases} \left[\left(v_s^{i-1}\right)^2 + \dfrac{3l_s C_d \rho_a^x}{2\rho_s d_s}\left(v_a^x - v_s^{i-1}\right)^2\right]^{1/2} & v_s^{i-1} \le v_a^x \\ \left[\left(v_s^{i-1}\right)^2 - \dfrac{3l_s C_d \rho_a^x}{2\rho_s d_s}\left(v_a^x - v_s^{i-1}\right)^2\right]^{1/2} & v_s^{i-1} > v_a^x \end{cases} \tag{19}$$

Based on the above equations, the flow chart to calculate shot velocity is given in Fig. 3.

To assess the model predictive capability, the shot peening conditions with six different types of shots were given in Tables 1 and 2. Steel shot is the most widely used material, zirconia shot has a smaller density than steel, and the density of tungsten carbide shot is almost twice as steel shot.

Figure 4 shows the effect of decay rate α on the calculated shot velocity. It can be seen that the variation of shot velocity out of the nozzle with the decay rate value is less than 10% within the peening distance of 50 mm. The longer the peening distance, the more significant of the decay rate on peening velocity. For a peening distance of 50 mm from the nozzle exit to the peening target, air flow velocity is always higher than shot velocity, so shot deceleration would not occur.

The effect of peening pressure on shot velocity is shown in Fig. 5. It can be seen that the peening pressure has a significant influence on shot velocity. Shot velocity increases dramatically with the increase of peening pressure which generates higher dragging force applied on a shot and results in a larger acceleration. It means that the model predictions are reasonable and reflect the physical phenomenon in shot peening.

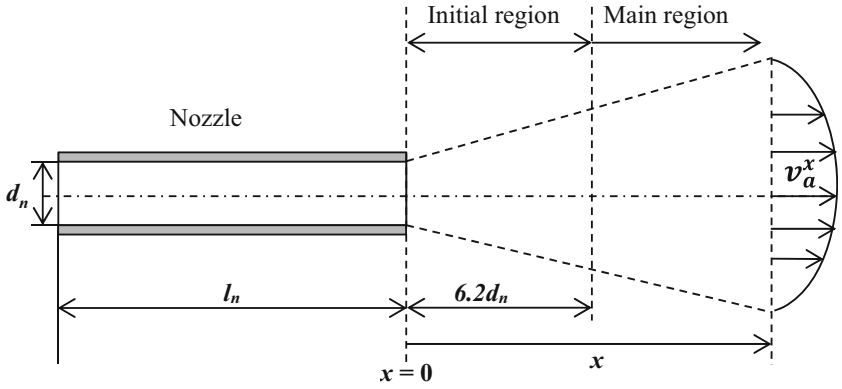

Fig. 2 Air-jet flow in free air (dimensions non-proportional)

Figure 6 shows the effect of shot properties on shot velocity. As shown in Eq. 8, for all types of shots, the shot acceleration decreases with the increase of shot diameter. For same shot material, the velocity of smaller diameter shots (0.356 mm) is higher than those of larger diameter shots (0.536 mm). The velocity difference is magnified at the high peening pressures in each case. It can also be seen that the velocity of zirconia shot is higher than that of steel shot. The velocity of tungsten carbide shot is the lowest among the three types of shot. It shows that for same shot size, high density reduces shot velocity.

Almen intensity of various shots under different peening pressures was calculated using the calculated shot velocity and the method developed by Miao et al. [12] as shown in Fig. 7. It can be seen that for same shot material, a larger shot produces higher Almen intensity, which is due to the larger drag force resulted from the larger cross section area of the shot. Thus, the kinetic energy of shot increases with the increase of shot diameter. A higher Almen intensity can be produced on the sample surface using a larger size shot under same peening condition.

For same shot size, Almen intensity of zirconia shots is very close to steel shots. However, Almen intensity of tungsten carbide shots is much higher than those of zirconia and steel shots for same shot size. It implies that the higher the Young's modulus, the higher Almen intensity. From the viewpoint of mechanics, higher Young's modulus produces less deformation, which allows more impact energy transferred to the workpiece.

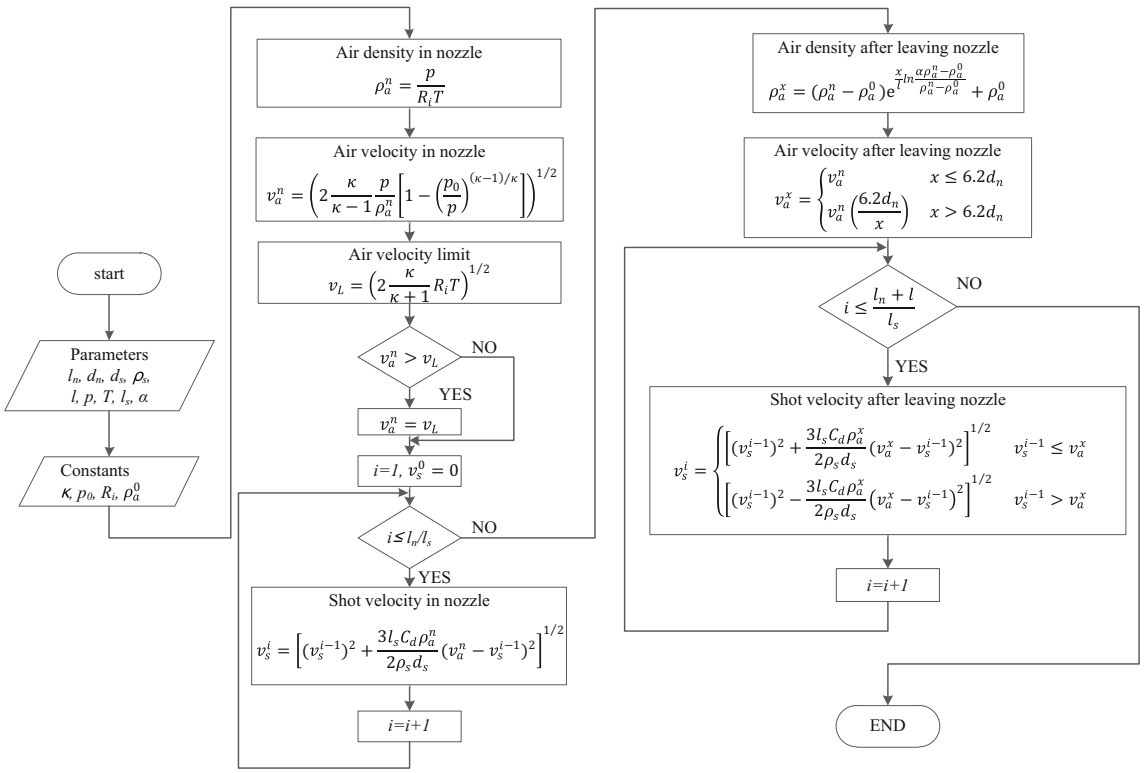

Fig. 3 Flow chart for the calculation of shot velocity

Table 1 Shot peening parameters for calculation

Distance to peening target l (mm)	50
Nozzle length l_n (mm)	50
Nozzle diameter d_n (mm)	5
Room temperature T (K)	300

3 Pressure-dependent plasticity modeling of ceramics

Ceramics plasticity in this study has been modeled with the Johnson-Holmquist 2 (JH-2) model. The JH-2 model is a phenomenological model which has been widely used to simulate the response of ceramics impacted at high velocity [24].

The JH-2 model consists of three main components: (1) a representation of the deviatoric strength of the intact and fractured material in the form of a pressure-dependent yield surface, (2) a damage model that transitions the material from the intact state to the fractured state, and (3) an equation of state (EOS) for the pressure-density relation that can include dilation (or bulking) effects. Each of these components of the model is described in the following sections. A physical explanation of damage and fracture in the JH-2 model is shown in Fig. 8.

The strength of the material is represented in terms of the normalized von Mises equivalent stress as:

$$\sigma^* = \sigma_i^* - D\left(\sigma_i^* - \sigma_f^*\right) \tag{20}$$

where σ_i^* is the normalized intact equivalent stress, D is damage variable. The normalized equivalent stress have the general form $\sigma^* = \sigma/\sigma_{HEL}$, where σ is the von Mises equivalent stress and σ_{HEL} is the equivalent stress at the Hugoniot elastic limit (*HEL*), at which a one-dimensional shock wave exceeds the elastic limit of material. The model assumes that the normalized intact and fractured stresses can be expressed as functions of pressure and strain rate as:

$$\sigma_i^* = A\left(P^* + T^*\right)^N \left(1 + C\ln\dot{\varepsilon}^*\right) \le \sigma_i^{\max} \tag{21}$$

$$\sigma_f^* = B\left(P^*\right)^M \left(1 + C\ln\dot{\varepsilon}^*\right) \le \sigma_f^{\max} \tag{22}$$

Table 2 Shot size and properties

Shot	Diameter (mm)	Material	Density ρ (kg/m^3)	Young's modulus E (GPa)	Poisson's ratio (ν)
S110	0.356	Steel	7.8×10^3	210	0.31
S170	0.504	Steel	7.8×10^3	210	0.31
Z300	0.356	Zirconia	3.85×10^3	300	0.27
Z425	0.504	Zirconia	3.85×10^3	300	0.27
W300	0.356	WC	15.8×10^3	550	0.23
W425	0.504	WC	15.8×10^3	550	0.23

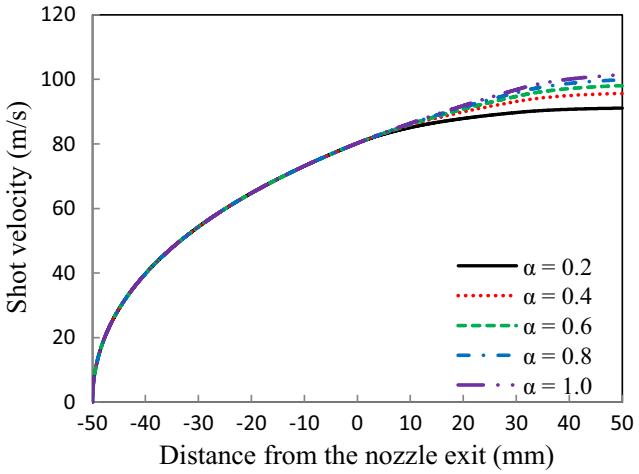

Fig. 4 Effect of air density decay rate on shot velocity (shot S110, p = 0.6 MPa)

The material constants are A, B, C, M, N, and the optional limits for the strengths are $\sigma_i^{\max}$ and $\rho_f^{\max}$. The normalized pressure is defined as $P^* = P/P_{HEL}$, where P is the actual pressure and P_{HEL} is the pressure at the HEL. Similarly, the normalized maximum tensile hydrostatic pressure $T^* = T/P_{HEL}$, where T is the maximum tensile hydrostatic pressure that the material can withstand.

The dimensionless strain rate is given as $\dot{\varepsilon}^* = \dot{\varepsilon}^p/\dot{\varepsilon}_0$, where $\dot{\varepsilon}^p$ is the equivalent strain rate and $\dot{\varepsilon}_0$ is the reference strain rate.

The material damage is based on a damage accumulation criterion that is similar to that in the Johnson-Cook fracture model. The damage parameter, D, accumulates with the plastic strain rate according to

$$D = \sum \frac{\Delta\varepsilon^p}{\varepsilon_p^f} \tag{23}$$

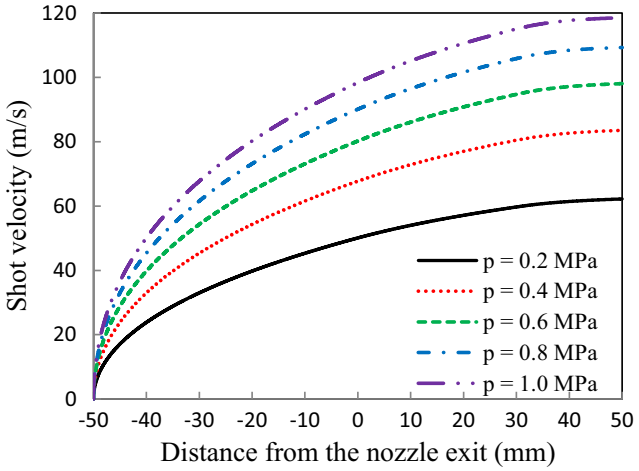

Fig. 5 Effect of peening pressure on shot velocity (shot S110, α = 0.6)

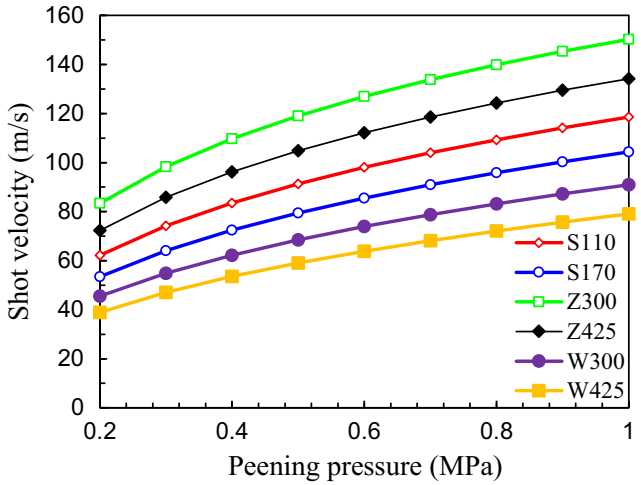

Fig. 6 Effect of shot properties on shot velocity

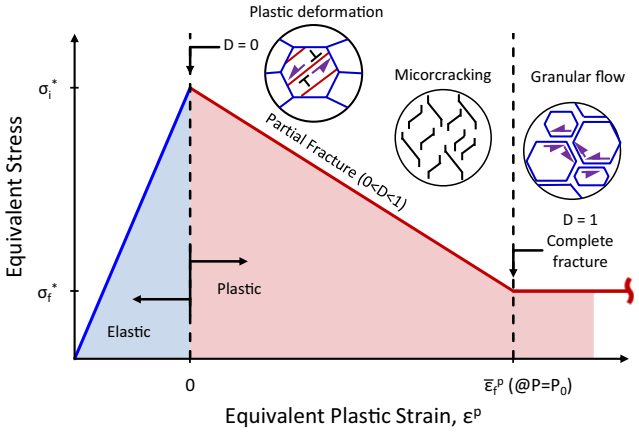

Fig. 8 Strength, damage, fracture, and element deletion under a constant pressure and strain rate

Here, $\Delta\varepsilon^p$ is the increment in equivalent plastic strain and ε_p^f is the equivalent plastic strain to fracture under constant pressure, defined as

$$\varepsilon_p^f = D_1\left(P^* + T^*\right)^{D_2}; \qquad \varepsilon_{p,min}^f \le \varepsilon_p^f \le \varepsilon_{p,max}^f \tag{24}$$

where D_1 and D_2 are the material constants. The optional parameters $\varepsilon_{p,\min}^f$ and $\varepsilon_{p,\max}^f$ are provided for additional flexibility to limit the minimum and maximum values of the fracture strain.

The pressure-density relationship is assumed to be given by an equation of state

$$P = \begin{cases} K_1\mu + K_2\mu^2 + K_3\mu^3 + \Delta P & \mu \ge 0 \\ K_1\mu & \mu < 0 \end{cases} \tag{25}$$

with $\mu = \frac{\rho}{\rho_0} - 1$

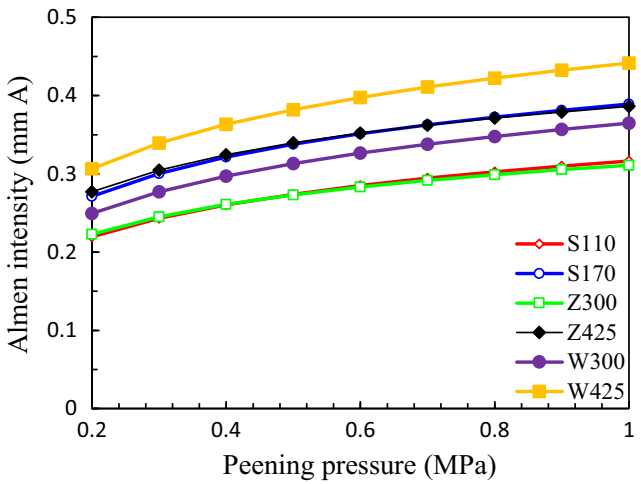

Fig. 7 Effect of peening pressure on Almen intensity

where K_1, K_2, K_3 are constants (K_1 is the initial bulk modulus), ρ is the current material density and ρ_0 is the reference density. ΔP is the additional pressure increment because of dilation (or bulking) that occurs when brittle materials fail.

The pressure increment is determined from energy considerations. The decrease in strength when the material undergoes damage (as it goes from an intact state to a failed state) produces a decrease in the deviatoric elastic energy, ΔU. This loss of elastic energy is converted into

Table 3 Material constants of the JH-2 model for Al_2O_3

Material	Al_2O_3
Density ρ (Kg/cm^3)	3700
Shear modulus G (GPa)	90.16
Strength constants	
A	0.93
B	0.31
C	0
M	0.6
N	0.6
$\dot{\varepsilon}_0$	1.0
T (GPa)	0.2
HEL (GPa)	2.79
P_{HEL} (GPa)	1.46
Damage constants	
D_1	0.005
D_2	1.0
Pressure-density relation constants	
K_1 (GPa)	130.95
K_2 (GPa)	0
K_3 (GPa)	0
β	1.0

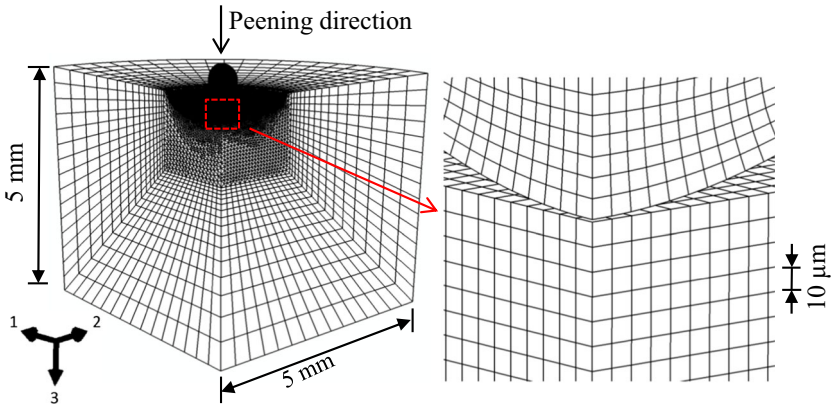

Fig. 9 Mesh of the shot peening simulation

potential hydrostatic energy by incrementally increasing ΔP according to

$$\Delta P_{t+\Delta t} = -K_1\mu_{t+\Delta t} + \sqrt{\left(K_1\mu_{t+\Delta t} + \Delta P_t\right)^2 + 2\beta K_1 \Delta U} \quad (26)$$

$$\Delta U = U(D) - U(D_{n-1}), U(D) = \frac{\sigma}{6G} \quad (27)$$

where β is the fraction of the elastic energy loss converted to potential hydrostatic energy ($0 \le \beta \le 1$).

The material constants of alumina for the JH-2 model are given in Table 3 [25].

4 Deformation mechanics in shot peening ceramics

4.1 Finite element simulation procedure

The mesh of the shot peening system is shown in Fig. 9. It should be highlighted that shot peening is random process. The workpiece is impacted with shots at random locations. However, this study was focused on the material deformation mechanisms of work material. Thus, a relatively simple shot peening model was created. The workpiece was impact five times at the same location. A quarter of the workpiece and shot was modeled because of the symmetry of geometry and loading. The workpiece was modeled as a cylindrical solid with a radius of 5 mm and thickness of 5 mm. The workpiece mesh was divided into two zones: a fine mesh zone with an element

Table 4 Simulation conditions

Case #	D_1	D_2	Workpiece material	Shot material	Shot diameter (mm)	Shot velocity (m/s)	Overlap ratio
1[a]	0.005	1	Al_2O_3	WC	0.65	15	–
2	0.0025	1	Al_2O_3	WC	0.65	15	–
3	0.01	1	Al_2O_3	WC	0.65	15	–
4	0.05	1	Al_2O_3	WC	0.65	15	–
5	0.1	1	Al_2O_3	WC	0.65	15	–
6	0.005	1	Al_2O_3	WC	0.65	15	20%
7	0.005	1	Al_2O_3	WC	0.65	15	50%
8	0.005	1	Al_2O_3	WC	0.65	15	80%
9	0.005	1	Al_2O_3	WC	0.65	7.5	–
10	0.005	1	Al_2O_3	WC	0.65	30	–
11	0.005	1	Al_2O_3	Stainless steel	0.65	21.35	–
12	0.005	1	Al_2O_3	WC	0.2	27.04	–
13	0.005	1	Al_2O_3	WC	0.4	19.12	–
14	0.005	1	Al_2O_3	WC	0.6	13.52	–
15	0.005	1	Al_2O_3	WC	0.8	9.75	–

[a] Baseline case

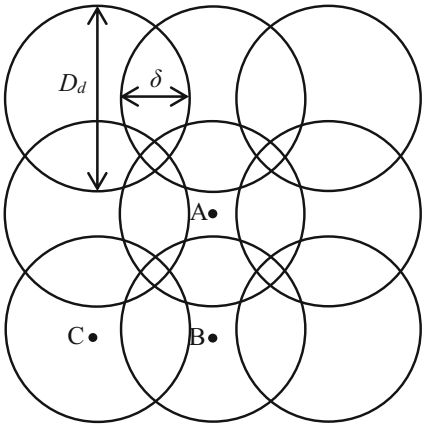

Fig. 10 Definition of overlap ratio

size of 10 μm in the impact region with a thickness of 150 μm and a radius of 1300 μm, and a relatively coarse mesh zone to model the other region away from region of impact. A gradual transition of element size from the fine mesh zone to the coarse mesh zone was used.

The bottom of workpiece was constrained in all directions. Symmetric boundary conditions were applied to the *XZ* and *YZ* planes of the mesh. An initial velocity calculated from the kinematic model was applied to the shot.

The workpiece Al_2O_3 was modeled using the JH-2 model. For simplicity, the shots were modeled as elastic. The tungsten carbide shots were given an elastic modulus E = 550 GPa, Poisson's ratio ν = 0.23, and density ρ of 15.8 × 10^3 kg/m^3. Stainless steel shots were given an elastic modulus E = 210 GPa, Poisson's ratio ν = 0.3, and density ρ of 7.8 × 10^3 kg/m^3. A Coulomb friction coefficient μ = 0.2 was defined between the shots and the workpiece.

The simulation conditions are given in Table 4. The effects of workpiece material property, shot velocity, shot diameter, shot material, and peening overlap ratio on residual stress were investigated. The overlap ratio was defined as the percentage of overlap (δ) among dent size which was determined from baseline case [26] (Fig. 10). The shots impact the work material at the same location for cases 1–5 and 9–15.

From Eq. 20, it can be seen that the failure strain is proportional to D_1. Thus, by varying the value of D_1, the effect of failure strain on mechanical behavior of ceramics under shot peening can be investigated. The shot velocity of baseline case was determined from the Almen intensity of 0.22 mmA based on the experiment condition [5]. The velocity for case 6–7 was calculated using the method given in Section 3.

4.2 Results and discussions

4.2.1 Data retrieving procedure

In order to investigate mechanism of ceramic plastic deformation and residual stress formation in multiple impacts, both instantaneous and residual strains/stresses were retrieved along the node path as shown in Fig. 11. The instantaneous strains/stresses were retrieved at the maximum plastic depth in each impact. The residual strains/stresses were retrieved at the fifth impact after shot bounced back.

4.2.2 Deformation behavior in single peening

Plastic deformation Figure 11 shows that the dent caused by plastic deformation in a single impact. The occurrence of plastic deformation has been verified by the high density dislocation in the subsurface of shot peened ceramics [3]. The radial stress σ_{11} in Fig. 12a shows that the maximum tensile stress reaches 200 MPa, which is much smaller than the tensile strength of alumina. Fracture is

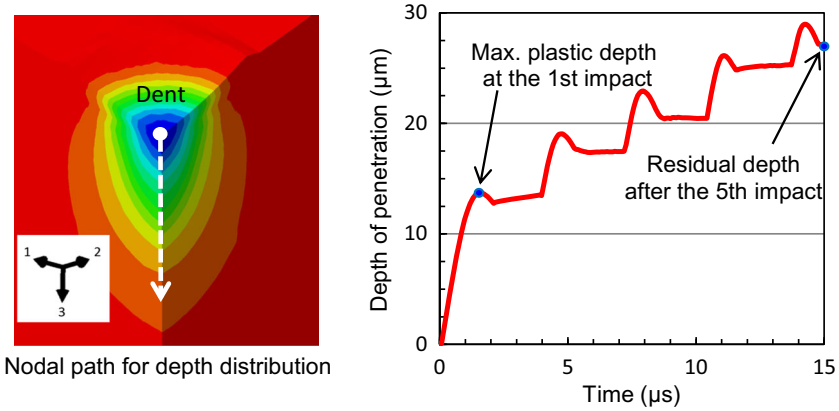

Fig. 11 Data retrieving path (quarter mesh)

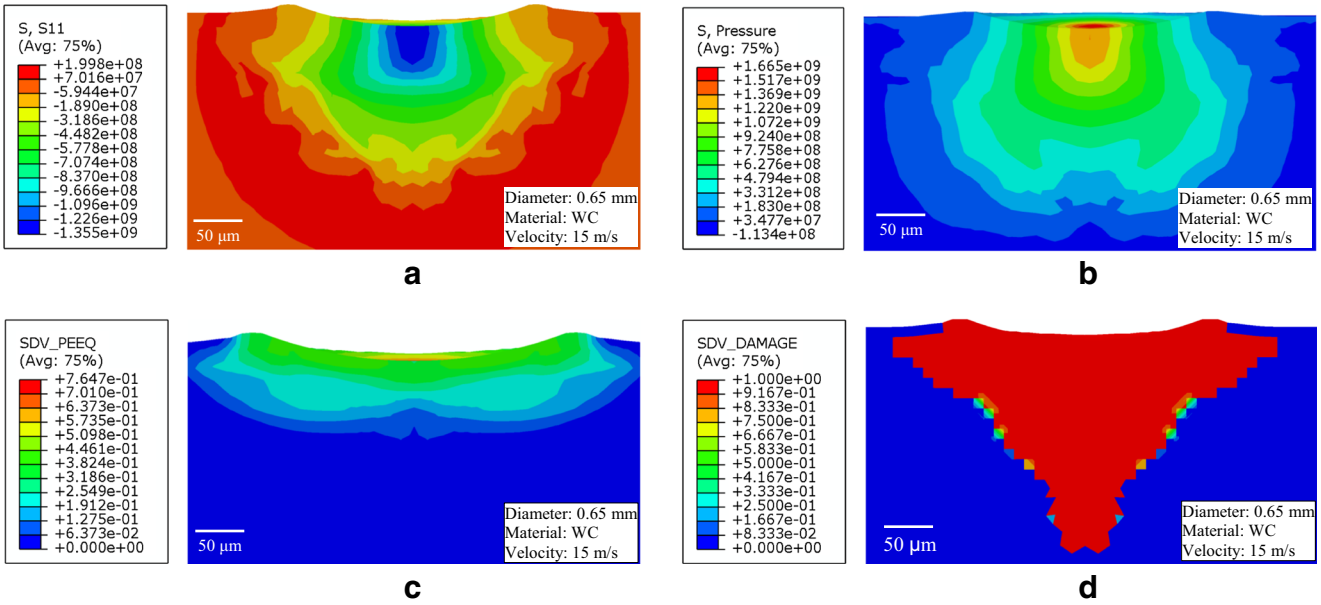

Fig. 12 **a** Radial stress σ_{11} in the baseline simulation case. **b** Pressure in the baseline simulation case. **c** Equivalent plastic strain PEEQ in baseline case. **d** Instantaneous damage in baseline case

unlikely to happen at such low stress. While the pressure in Fig. 12b is as high as 1.67 GPa. In the JH-2 model, the failure strain is highly dependent on pressure. With such high pressure, ceramics will undergo significant plastic deformation before PEEQ reaches failure strain. From the viewpoint of fracture mechanics, a high pressure will suppress crack propagation and makes the ceramics more ductile, which is demonstrated in the corresponding equivalent plastic strain PEEQ in Fig. 12c. It can be seen that the maximum PEEQ is on the top surface.

Damage evolution As shown in Fig. 12d, the impact creates a "damaged" zone of about 200 μm depth. In the JH-2 model, "damage" is defined as a state variable to represent the strength degrading. From Eqs. 20–22, it can be seen that the material strength decreases with the increase of damage. When the "damage" value exceeds one, it means the material cannot withstand any tensile loading according to Eqs. 20–22. It means that the microcracks coalesce and the material transitions into a granular medium comprising narrowly separated granules. It can be seen from Fig. 12d that the damage of most elements in the damaged zone reaches one. According to Deshpande et al. [27], there are three inelastic deformation mechanisms for ceramics under indentation or impact: (i) lattice plasticity due to dislocation glide or twining, (ii) microcracking extension, and (iii) granular flow of densely packed communited particles. The increase of damage can be interpreted as the growth of microcracks. Thus, it is reasonable to conclude that the "damage" zone introduced by shot peening was caused by microcracks extension. The existence of microcracks was confirmed by TEM of shot peened ceramics subsurface by Moon et al. [3].

Residual stress distribution The residual stress σ_{11} of baseline case is shown in Fig. 13. It can be observed that the maximum compressive residual stress is up to −0.9 GPa at 180 μm below the top surface, while the residual stress on the top surface is very low. That is because when a shot is bounced back, the external pressure applied by the shot is also gone. Thus, the pressure in elements at top surface will be very low. In the JH-2 model, the strength decreases as the pressure decreases.

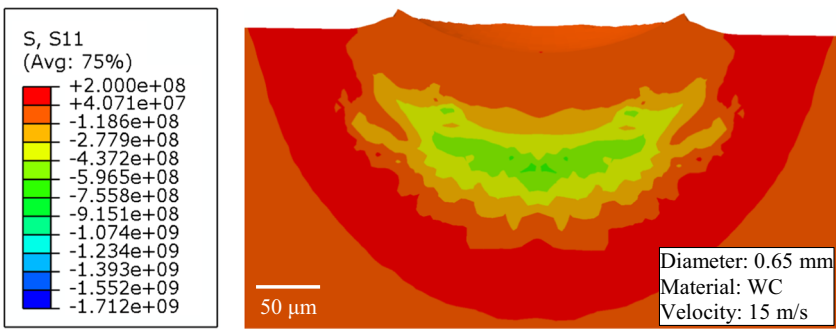

Fig. 13 Residual stress σ_{11} contour of baseline case

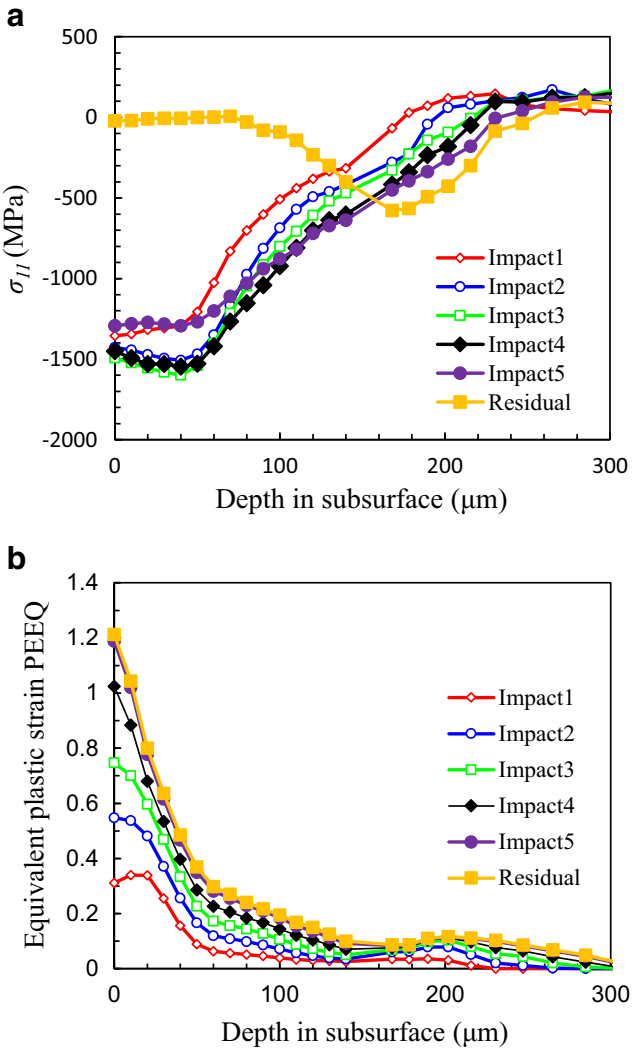

Fig. 14 **a** Distribution of stress σ_{11} in baseline case. **b** Distribution of equivalent plastic strain PEEQ in baseline case

Thus, those elements at top surface can withstand very low stress. The depth distribution of stress and strain is shown in Fig. 14. The stress and strain increases as the number of impacts increases. However, the stress value becomes saturate after three impacts. The stress magnitude reduction from impact 4 to impact 5 may be explained by the increased damage in the work material. The damaged material can withstand lower stress than the intact material. The residual stress profile forms a hook shape, and the maximum compressive residual stress occurs at about 180 μm depth in the subsurface.

4.2.3 Deformation behavior in multiple peening

Effect of material constants Material damage constant D_1 has more influence than constant D_2 on plastic failure strain according to Eq. 24. The effect of damage constant D_1 is shown in Fig. 15. It can be seen that the instantaneous stress

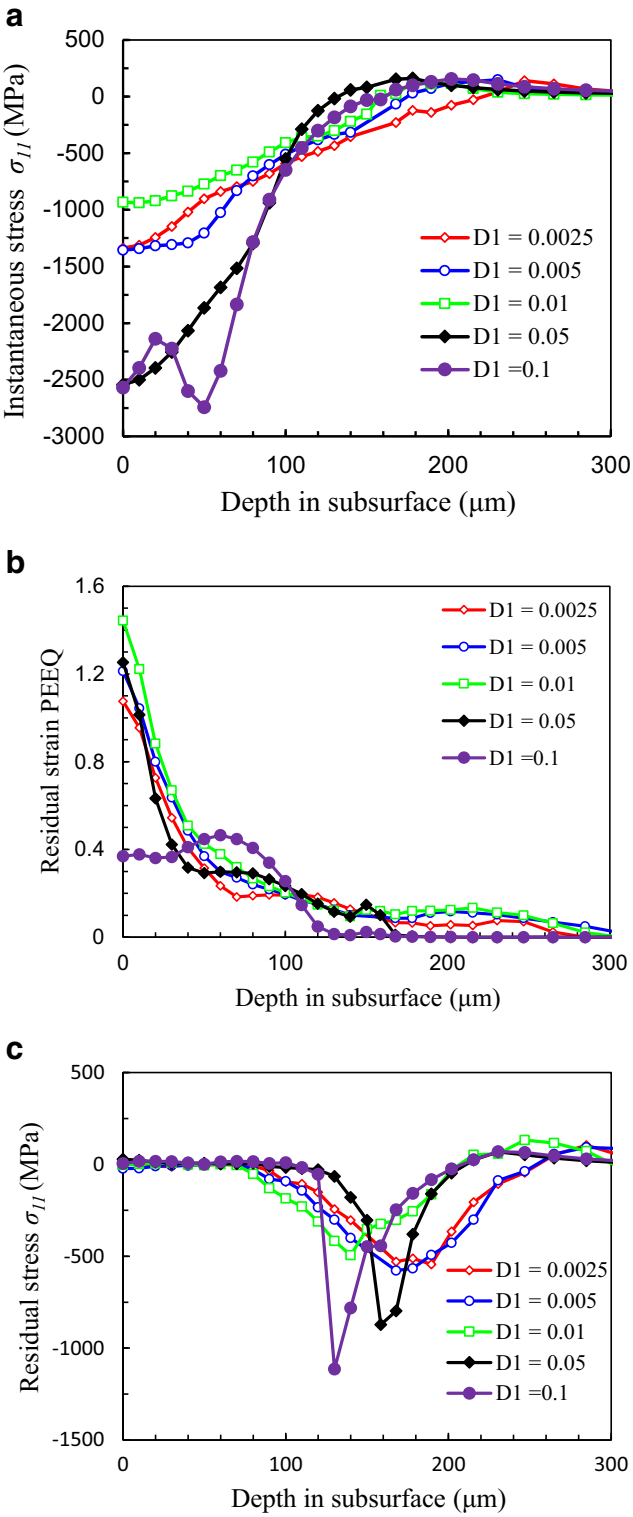

Fig. 15 **a** Effect of damage constant on stress. **b** Effect of damage constant on residual strain PEEQ. **c** Effect of damage constant on residual stress

increases with the increasing D_1 (Fig. 15a). With the increase of D_1 from 0.0025 to 0.01, the material will undergo more plastic deformation before failure as shown in Fig. 15b. The

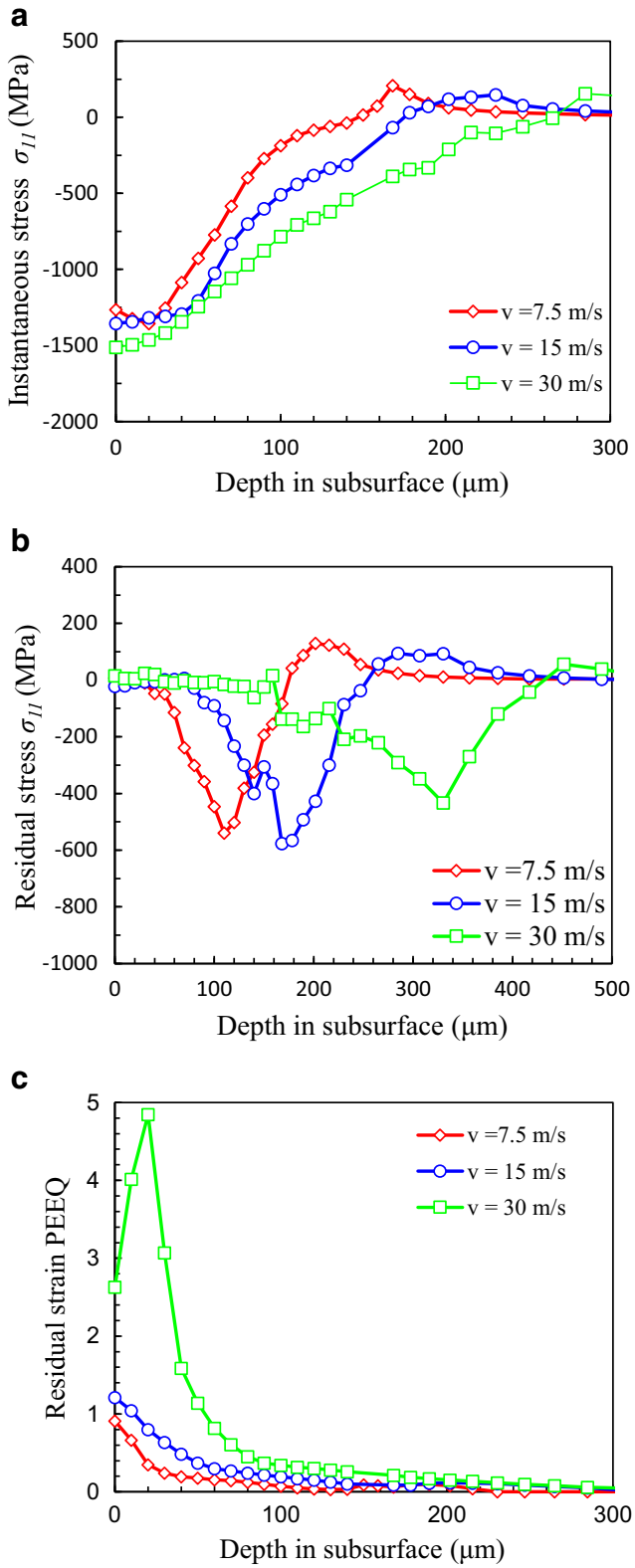

Fig. 16 **a** Effect of shot velocity on instantaneous stress. **b** Effect of shot velocity on residual stress. **c** Effect of shot velocity on residual strain PEEQ

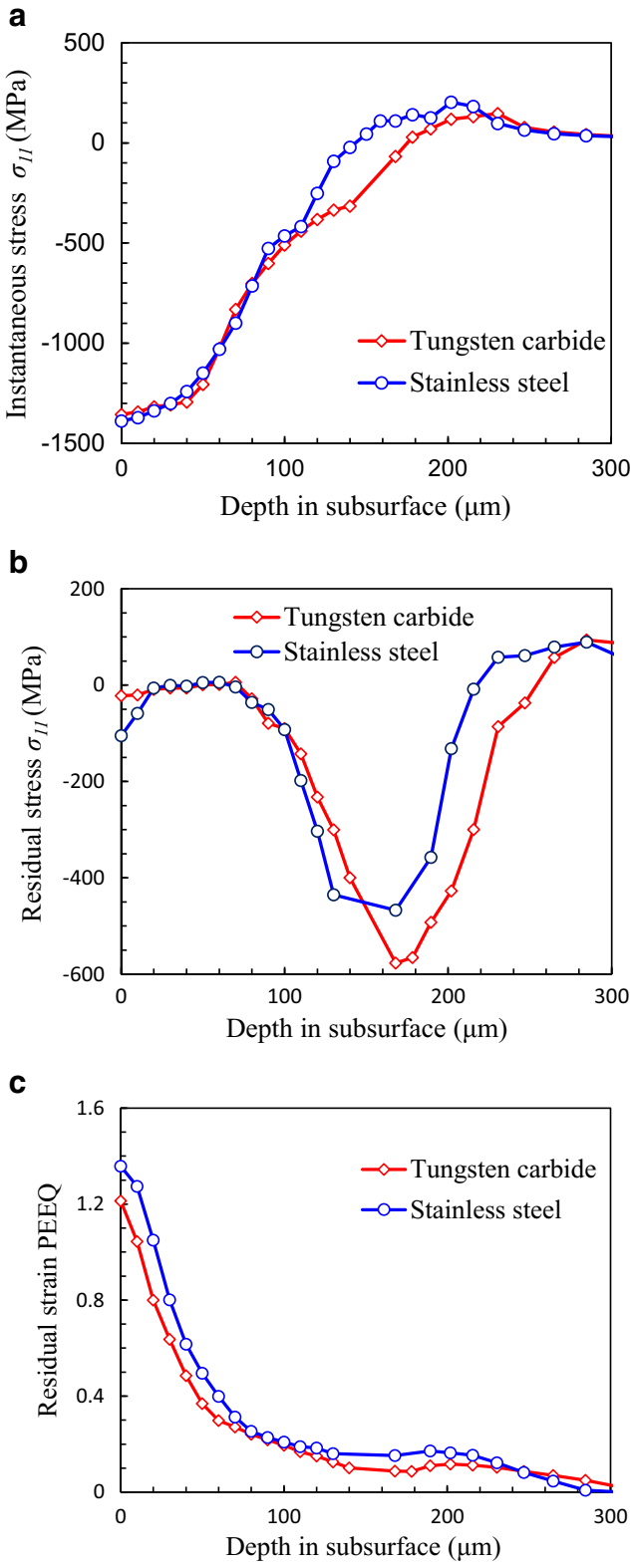

Fig. 17 **a** Effect of shot material on instantaneous stress. **b** Effect of shot material on residual stress. **c** Effect of shot material on residual strain PEEQ

non-damaged elements in the plastic deformation zone will withstand higher loading than the damaged elements. Thus, the instantaneous stress increases with the increase of D_1. However, the further increase in D_1 (D_1 = 0.05 and 0.1)

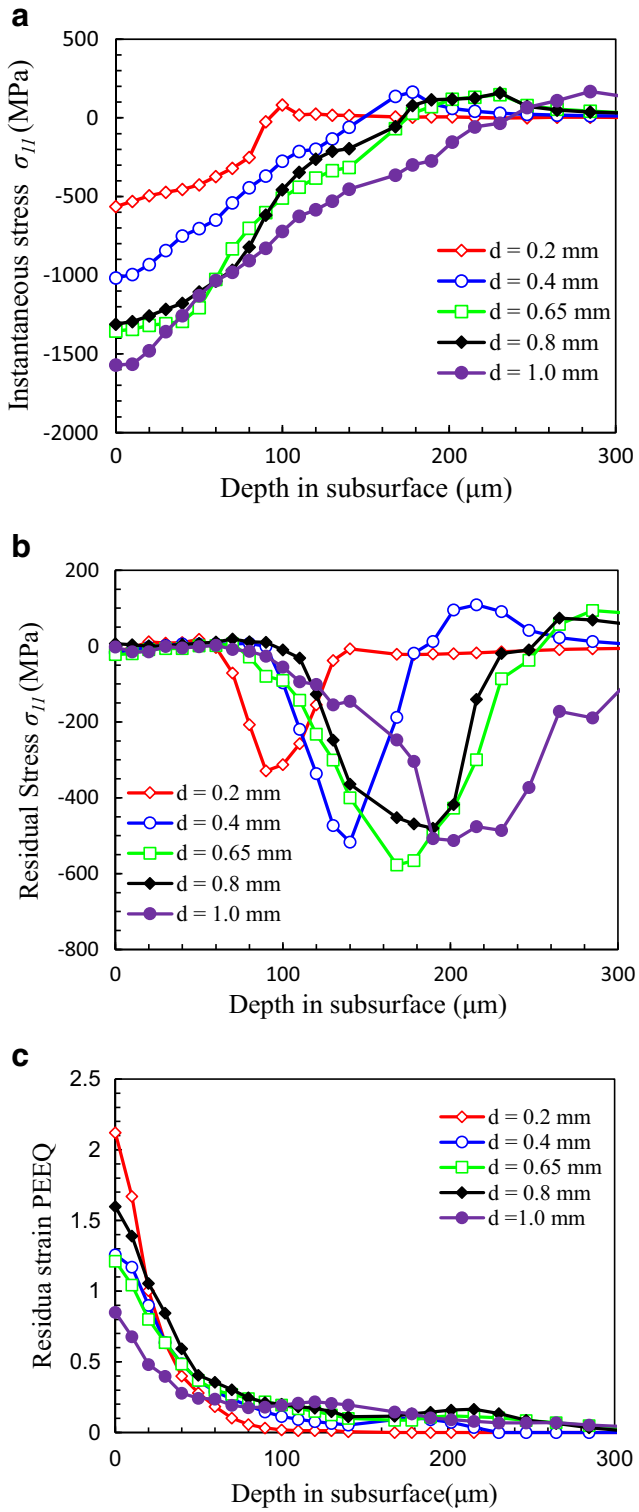

Fig. 18 **a** Effect of shot diameter on instantaneous stress. **b** Effect of shot diameter on residual stress. **c** Effect of shot diameter on residual strain PEEQ

reduces the residual plastic strain, which can be explained by the higher yield stress due to the less damage with higher D_1 (shown in Fig. 8). Figure 15c shows that residual stress also increases with the increase of D_1 due to the increased plastic deformation zone.

Effect of shot velocity Figure 16 shows that the shots with higher velocity generate a larger stress in the workpiece. The stress decreases to zero at about 200 μm in the subsurface for peening velocity 7.5 and 15 m/s, while it increases to 250 μm for higher velocity 30 m/s. That shows that the depth of compressive layer (Fig. 16b) also increases with shot velocity. Figure 16c shows that higher peening velocity generates higher plastic deformation, which explains the stress is also higher for higher peening velocity.

Effect of shot material The stress and strain for shots with different shot materials are compared in Fig. 17. The instantaneous stress is nearly equivalent for WC and steel shots (Fig. 17a). The residual stress induced by WC shots is higher than the stainless steel shot (Fig. 17b). This beneficial effect could be attributed to the higher peening energy carried by the higher density shots. However, the effect of shot material is manifested by a coupling effect of density and Young's modulus. The residual PEEQ is higher for steel shots, which may be explained by the fact that under the same peening pressure steel shots have higher velocity due to the smaller density (Fig. 17c).

Effect of shot size The effect of shot diameter is shown in Fig. 18. Since the kinematic energy increases with the cross sectional area of the shot, a larger diameter shot will impact higher deformation energy into the workpiece and generate larger instantaneous stress in Fig. 18a. As expected, a larger depth of compress stress layer is produced as shown in Fig. 18b. However, the residual PEEQ at the surface for smaller shots is larger than the larger shots, but the depth is shallower (Fig. 18b).

Effect of overlap ratio The depth distribution of stress for case 13 (overlap ratio = 20%) at different locations depicted in Fig. 10 is shown in Fig. 19a. It can be seen that stress at location A is much higher than stress at B and C. The difference in residual stress at different locations shows that when the coverage is low, the residual stress distribution tends to be non-uniform. The stress and strain at location A for different overlap ratios are shown in Fig. 19b–d. It can be seen that residual stress for high overlap ratio are higher than that for low overlap ratio. This is consistent with the experimental finding that the longer shot peening time leads to higher residual stress [5]. The max. *PEEQ* is identified in the subsurface in the case of 80% overlap. Similar behavior is also observed in Fig. 16c at high shot velocity, which can be explained by the increased damage in surface layer induced by higher shot velocity or higher overlap ratio. The damaged surface layer material can withstand lower stress/strain than the intact material.

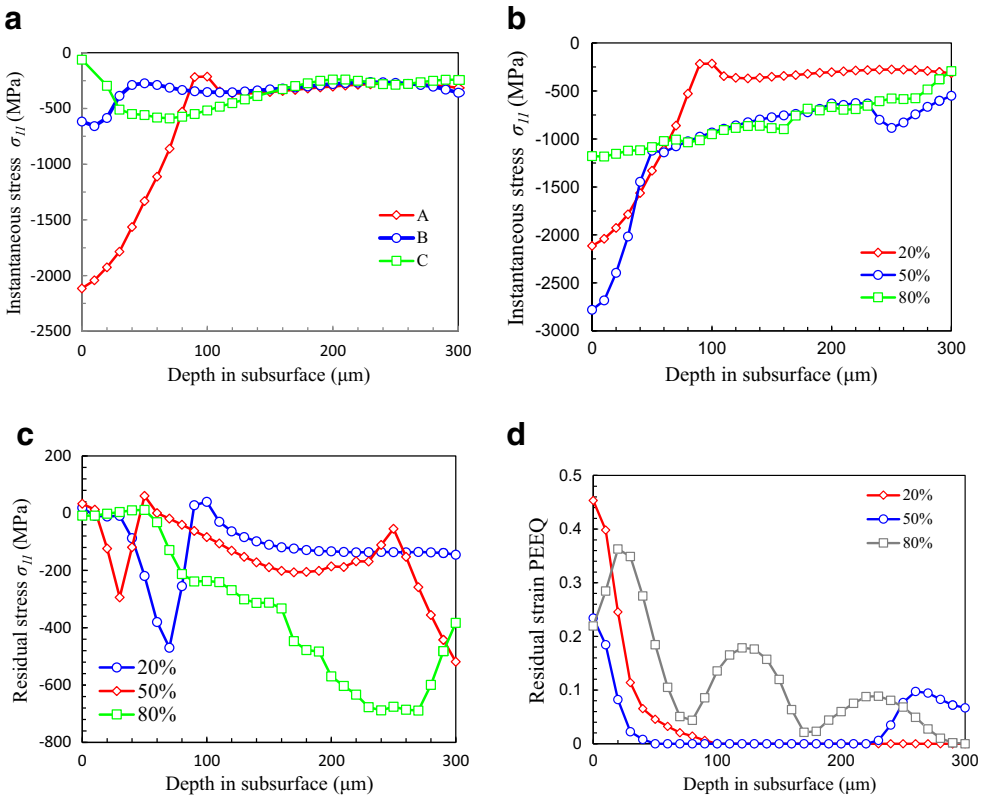

Fig. 19 **a** Instantaneous stress at different locations for overlap ratio = 20%. **b** Effect of overlap ratio on instantaneous stress. **c** Effect of overlap ratio on residual stress. **d** Effect of overlap ratio on residual strain PEEQ

5 Conclusions

This study focused on the development of kinematic model and deformation mechanics in shot peening of ceramic Alumina. A 3D finite element simulation model has been developed to investigate the effect of multiple peening on ceramic deformation (stress, pressure, strain, material damage, and residual stress). The effects of material damage parameter, peening velocity, shot material, shot diameter, and peening overlap ratio were analyzed. The key results are summarized as follows:

- A kinematic model has been developed and numerically implemented to calculate the shot velocity with improved accuracy by accounting for air drag and density variation outside of peening nozzle. At higher peening pressure, the air drag force increases with the peening pressure.
- Almen intensity depends on the shot kinematic energy and shot material properties. Shots with higher Young's modulus generate higher Almen intensity and larger compressive residual stress.
- Compressive residual stress was predicted and confirmed with the experimental data. Residual stress increases with the increasing failure strain.
- Higher peening velocity generates large plastic deformation and larger residual stress. WC shot generates higher residual stress than steel shot. Residual stress increases with increase of overlap ratio.
- The material damage of the peened ceramics is induced by microcracks, which has a significant influence on the distribution of residual stress.

Acknowledgements The research was partially supported by the Chinese Education Council Fellowship (#201206220032) and Shandong Taishan Scholar Program.

References

1. Ferraris E, Vleugels J, Guo YB, Bourell D, Kruth JP, Lauwers B (2016) Shaping of engineering ceramics by electro, chemical and physical processes. CIRP Ann Manuf Technol 65(2):761–784
2. Pfeiffer W, Frey T (2002) Shot peening of ceramics: damage or benefit? CFI-Ceramic Forum Int 79(4):E25–E28
3. Moon W, Ito T, Uchimura S, Saka H (2004) Toughening of ceramics by dislocation sub-boundaries. Mat Sci Eng A-Struct 387–389:837–839
4. Tomaszewski H, Godwod K, Diduszko R, Carrois F, Duchazeaubeneix J (2006) Shot peening—a new method for improving mechanical properties of structural ceramics. Key Eng Mater 317:277–280
5. Pfeiffer W, Frey T (2006) Strengthening of ceramics by shot peening. J Eur Ceram Soc 26(13):2639–2645
6. Takahashi K, Nishio Y (2012) Improvement of the contact strength of Si_3N_4/SiC by a combination of shot peening and crack-healing. JSME Int J Ser A 6(2):144–153
7. Tanaka K, Akiniwa Y, Morishita Y (2005) Residual stress distribution in the sub-surface region of shot-peened ceramics. Transe Jpn Soc Mech Eng 71:1714–1721

8. Takahashi K, Nishio Y, Kimura Y, Ando K (2010) Improvement of strength and reliability of ceramics by shot peening and crack healing. J Eur Ceram Soc 30(15):3047–3052
9. Kirk D (2007) Generation of air-blast shot velocity. Shot Peener 21(1):24–30
10. Li HZ, Wang J, Fan JM (2009) Analysis and modelling of particle velocities in micro-abrasive air jet. Int J Mach Tool Manu 49(11): 850–858
11. Almen J, Black JPH (1963) Residual stresses and fatigue in metals. McGraw-Hill
12. Miao HY, Larose S, Perron C, Lévesque M (2010) An analytical approach to relate shot peening parameters to Almen intensity. Surf Coat Tech 205(7):2055–2066
13. Al-Obaid YF (1990) Three-dimensional dynamic finite element analysis for shot-peening mechanics. Comput Struct 36(4):681–689
14. Meguid S, Shagal G, Stranart J (2007) Development and validation of novel FE models for 3D analysis of peening of strain-rate sensitive materials. J Eng Mater-T ASME 129(2):271–283
15. Kim T, Lee H, Kim M, Jung S (2012) A 3D FE model for evaluation of peening residual stress under angled multi-shot impacts. Surf Coat Tech 206(19–20):3981–3988
16. Hong T, Ooi JY, Shaw BA (2008) A numerical study of the residual stress pattern from single shot impacting on a metallic component. Adv Eng Softw 39(9):743–756
17. Miao HY, Larose S, Perron C, Lévesque M (2009) On the potential applications of a 3D random finite element model for the simulation of shot peening. Adv Eng Softw 40(10):1023–1038
18. Frija M, Hassine T, Fathallah R, Bouraoui C, Dogui A (2006) Finite element modelling of shot peening process: prediction of the compressive residual stresses, the plastic deformations and the surface integrity. Mat Sci Eng A-Struct 426(1–2):173–180
19. Bagherifard S, Ghelichi R, Guagliano M (2012) Numerical and experimental analysis of surface roughness generated by shot peening. Appl Surf Sci 258(18):6831–6840
20. Gangaraj SMH, Guagliano M, Farrahi GH (2014) An approach to relate shot peening finite element simulation to the actual coverage. Surf Coat Tech 243:39–45
21. Thomas PJ (1999) Simulation of industrial processes for control engineers. Butterworth-Heinemann
22. Momber A (2008) Blast cleaning technology. Springer
23. Rajaratnam N (1976) Turbulent Jets. Elsevier
24. Johnson GR, Holmquist TJ (1994) An improved computational constitutive model for brittle materials. High-pressure science and technology, Colorado Springs, CO, USA, AIP Conference Proceedings
25. Anderson C, Johnson G, Holmquist T (1995) Ballistic experiments and computations of confined 99.5% Al_2O_3 ceramic tiles. Proceedings of the 15th International Symposium on Ballistics, Israel, Jerusalem.
26. Guo YB, Sealy MP, Guo C (2012) Significant Improvement of corrosion resistance of biodegradable metallic implants processed by laser shock peening. CIRP Ann Manuf Technol 61(1):583–586
27. Deshpande VS, Gamble EAN, Compton BG, McMeeking RM, Evans AG, Zok FW (2011) A constitutive description of the inelastic response of ceramics. J Am Ceram Soc 94:s204–s214